GKSS
FORSCHUNGSZENTRUM
in der HELMHOLTZ GEMEINSCHAFT

Simulation of the climate of the last five centuries

Authors:

E. Zorita
H. von Storch
F. J. Gonzales-Rouco
U. Cubasch
J. Luterbacher
S. Legutke
I. Fischer-Bruns
U. Schlese

ISSN 0344-9629

GKSS 2003/12

GKSS 2003/12

Simulation of the climate of the last five centuries

Authors:

E. Zorita
H. von Storch
(Institute for Coastal Research, GKSS Research Centre, Geesthacht, Germany)

F. J. Gonzalez-Rouco
(Universidad Complutense, Depto. de Astrofisica y CC. de la Atmosfera, Madrid, Spain)

U. Cubasch
(Institute of Meteorology, Freie Universität Berlin, Berlin, Germany)

J. Luterbacher
(National Center of Competence in Research on Climate, University of Bern, Bern, Switzerland)

S. Legutke
I. Fischer-Bruns
U. Schlese
(Model & Data Group, Max-Planck-Institute of Meteorology, Hamburg, Germany)

GKSS-Forschungszentrum Geesthacht GmbH • Geesthacht • 2003

Die Berichte der GKSS werden kostenlos abgegeben.
The delivery of the GKSS reports is free of charge.

Anforderungen/Requests:

GKSS-Forschungszentrum Geesthacht GmbH
Bibliothek/Library
Postfach 11 60
D-21494 Geesthacht
Germany
Fax.: (49) 04152/871717

Als Manuskript vervielfältigt.

ISSN 0344-9629

GKSS-Forschungszentrum Geesthacht GmbH · Telefon (04152)87-0
Max-Planck-Straße · D-21502 Geesthacht / Postfach 11 60 · D-21494 Geesthacht

GKSS 2003/12

Simulation of the climate of the last five centuries

Eduardo Zorita, Hans von Storch, Fidel J. Gonzalez-Rouco, Ulrich Cubasch, Juerg Luterbacher, Stephanie Legutke, Irene Fischer-Bruns and Ulrich Schlese

43 pages with 15 figures

Abstract

In a transient climate simulation of the last 500 years with a coupled atmosphere-ocean model driven by estimated solar variability, volcanic activity and atmospheric concentrations of greenhouse gases for the last centuries, the model simulates a climate colder than present conditions almost globally, and the degree of cooling is larger than most empirical reconstructions. The model simulates two clear minima of the global mean temperature around 1700 A.D. (the Late Maunder Minimum) and around 1820 A.D. (the Dalton Minimum). The temperature trends simulated after the recovery from these minima are as large as the observed warming in the 20th century. Additionally, in the Late Maunder Minimum the simulated temperature field in Europe agrees well with empirical reconstructions from proxy-data, with an intense drop of air-temperature in the North Atlantic ocean, an extensive sea-ice cover south of Greenland, lower salinity in North Atlantic at high latitudes, and reduced intensities of the Golf Stream and the Kuroshio Stream.

Simulation des Klimas der letzten fünf Jahrhunderte

Zusammenfassung

Eine Klimasimulation der letzten fünfhundert Jahre mit einem gekoppelten Atmosphären-Ozean-Modell zeigt globale Temperaturen, die kälter als der heutige Zustand und auch kälter als die meisten empirischen Klimarekonstruktionen für diese Periode sind. Das Modell simuliert zwei deutige Temperaturminima um 1700 A.D. (Spätes Maunder Minimum) und um1820 A.D. (Dalton Minimum). Der Temperaturanstieg nach diesen Minima erreicht ähnliche Werte wie sie im 20. Jahrhundert beobachtet worden sind. Im Späten Maunder Minimum stimmt die räumliche Verteilung der Temperaturabweichungen in Europa mit der aus empirischen Rekonstruktionen überein, mit einer deutlichen Abkühlung im Nordatlantik, einer ausgedehnten Meereisbedeckung, niedrigerem Salzgehalt in den hohen Breiten des Nordatlantiks und schwächeren Golf- und Kuroshiostrom.

Manuscript received / Manuskripteingang in TDB: 1. April 2003

Contents

1 Introduction

The climate of the last thousand years has recently received considerable attention (Mann et al., 1999; Jones et al, 2001; Esper et al., 2002), with the long-term goal of estimating the level of natural variability in the absence of large anthropogenic influences. This level of natural variability, either caused by the internal dynamics of the climate system or induced by variations in the external forcing, forms the framework in which the global tropospheric warming observed in the 20^{th} century has to be interpreted. Although the evidence of an anthropogenic influence on the global climate due to the increase of atmospheric greenhouse gas concentrations is strengthening (IPCC, 2001), It is also acknowledged that uncertainties in the typical range of natural climate variations at timescales of centuries still exist. Since the temperature instrumental record is only about 150 years long, an estimation of the natural temperature variations has to be based on climate proxy indicators. In the last years several attempts have been carried out to reconstruct global or hemispheric temperatures in the last centuries with annual or decadal resolution. The best known is perhaps the reconstruction by Mann et al (1999, hereafter MBH99), based partly on a multiproxy dataset, comprising tree-ring, coral, long instrumental, and ice core records. Other reconstructions based on dendrochronological records have been also published recently (Briffa et al., 2001;Esper et al, 2002; Jones et al, 1998). Also, bore-hole temperature measurements have been shown to contain information of past surface temperatures, that can be retrieved by analyzing the current temperature profile up to about 500 m depth (Huang et al, 2000). Many other continuous reconstructions of regional character, not only for temperature but also for other variables, such as precipitation and wind, can be found in the literature. They can be based on other type of proxy indicators, such as documentary historical evidence, concentrations of certain metals in terrestrial sediments, analysis of stalagmites growth, among others.

In general, the empirical climate reconstruction of the last few centuries identify periods of widespread temperatures lower than today that lasted until about 1850. This period is known as the Little Ice Age (LIA). These lower temperatures reached a minimum around the so called Late Maunder Minimum (LMM; around 1680 to 1710) as shown by many European and Asian indicators, a period in which the sun activity, as estimated from the number of sun spots, was reduced (Eddy, 1976). Also in this period an increased volcanic activity is believed to have occurred (Briffa et al. 1999). The LMM, however, does not seem to be restricted to the European

region, and other proxy indicators located in other parts of the world also indicate minimum temperatures in these decades (Fritts and Low, 1985; Druffel and Griffin, 1993; Dunbar and Cole, 1993; Quin et al., 1998; Holmgren et al., 1999; Tyson et al., 2000; Wang et al., 2001; Villalba et al., 2002; Yang et al., 2002; Ge et al.,). The LIA followed a period of warmer temperatures, the so called Medieval Warm period, in which global temperatures could have attained the levels of the 20^{th} century (Jones et al., 2001).

The different empirical reconstructions disagree somewhat on the level of cooling in the LIA, and in particular during the LMM. In the temperature reconstructions MBH99, based on a comprehensive multiproxy dataset from both the extratropical and tropical regions, the coldest decade was 1696-1705 over the NH, with 0.35K lower annual temperatures relative to the 1902-1980 mean. On the other hand, the North Hemisphere (NH) temperature reconstructions by Jones et al. (1998, hereafter JBBT) or Esper et al. (2002, hereafter ECS), based on a smaller number of proxy locations (17 and 14, respectively) of mostly dendrochronological time series indicate colder conditions through the LIA, of roughly 0.5 K and 0.7 K colder than the 1902-1980 mean, respectively. Due to the extensive use of dendrochronological data these three NH reconstructions are probably reflecting more strongly temperature deviations in the extratropical tree-growing season. Finally, temperature estimations based on borehole measurements (Huang et al, 2000) are able to yield past temperature trends on a centennial time scale. These also indicate global temperatures about 0.7 K colder than the 20th century mean. However, these reconstructions based on borehole temperature measurements have been recently questioned by Mann et al. (2003).

It has to be noted that these reconstructions have not targeted the same variable, either the annual or seasonal, global, Northern hemispheric, or hemispheric extratropical temperatures. For this reason a straightforward comparison among them is not easy. One strategy to by-pass this problem has been to rescale the reconstructions using proportionality factors derived from the interannual observational record (Briffa and Osborn, 2002), thereby assuming that these factors remain unchanged in other climate conditions and at much longer timescales. This assumption, though reasonable, is not easy to check and it has been questioned (Mann and Hughes, 2002; Esper and Cook, 2002)

On the modeling side, the research effort has been more limited to date. A climate simulations of the LMM with an atmospheric General Circulation Model coupled to a slab ocean model with frozen LMM external forcing (Shindell et al, 2001) has been carried out. A transient

simulation with an energy balance climate model has been also recently published (Crowley, 2000). Quite recently, a simulation of the last millennium with a two-dimensional zonally averaged atmosphere-ocean model has been presented (Betrand et al., 2002). Transient experiments with fully coupled OAGCMs have only been run so far for the last 300 years (Cubasch et al, 1997; Hegerl et al, 1997, Cubasch and Voss, 2000). They show that the minimum of radiative forcing during the Dalton Minimum could cause a global cooling. Other transient experiments started in the middle of the 19^{th} century to investigate the question whether mankind or natural causes have been responsible for the observed climate change (Stott et al., 2000).

The level of LIA cooling in the Crowley (2000) simulation broadly agrees with the MBH99 reconstruction. The level of warming reconstructed and simulated in the last century is much larger than the typical temperature variations in the last millenium, so that the possible anthropogenic influence comes out very clearly (IPCC, 2001). In the series of simulations by Bertrand et al. (2002), in which the influence of the different external factors is investigated, the global warming observed in the last 150 years can be only explained when all these factors are considered simultaneously. However, the level of climate variability in the previous centuries can be coherently explained by the action of solar and volcanic activity (Betrand et al., 2002). In both models, however, the model sensitivity to variations in external forcing has been controlled by a parameter that can be tuned to better reproduce the simulations in the instrumental period.

The physical mechanisms for the centennial climate variations are much more difficult to identify in empirical reconstructions or in simplified models. These can in effect point out to statistical correlations between external factors and global or hemispheric temperatures. The analysis of more comprehensive models can give insights to unveil the physical mechanisms operating in nature. The simulations by Cubasch and Voss (2000) indicate that a reduced solar radiation can explain the degree of cooling during the Dalton Minimum. The simulation by Shindell et al. (2001) suggested a physical mechanisms for the intensification of these colder conditions aroung the LMM in the European region. This mechanism is related to the reaction of the low-stratospheric circulation to a weaker insolation and to an associated weakening of the winter zonal circulation at midlatitudes in the North Hemisphere, i.e. a weakened North Atlantic Oscillation (Luterbacher et al. 2002b). A version of the same model used by Shindell et al. (2001) without a realistic stratosphere fails to simulate the extreme cold conditions in the LMM.

A transient climate simulation with a state-of-the art climate model represents a contribution to clarify the discrepancies of some of the climate reconstructions presented so far and to identify mechanisms that may amplify or reduce the effect of the varying external forcing. For instance, a fully dynamical ocean model can better represent changes in oceanic heat transport and in the ocean-atmosphere feedback process than energy balance models or models with a slab ocean can do. However, it has to be kept in mind that simulations performed with other climate models, and perhaps with refined external forcing may differ from the results presented here, so that a conclusive answer to this question will probably be reached by an extensive comparison of different paleoreconstructions and paleosimulations. In other words, the disagreement between the simulation described in this paper and other future simulations might be as large as the divergence in the empirical reconstructions.

The paper is structured as follows: in section 2 a short description of the model and the external forcing is presented. Section 3 is focused on the main results of the simulation on a global or hemispheric scale. In a comprehensive climate simulation as this, many different aspects can be considered for analysis. Here, only some important global aspects of the simulation, and their comparison with available climate reconstructions, are considered: the variability of the global temperature at decadal and centennial timescales and several reconstructions of the North Atlantic Oscillation. Section 4 of the paper is devoted in more detailed to the Late Maunder Minimum. The simulated West European temperatures are compared to an empirical reconstruction based on a multiproxy dataset, dense enough to yield spatially resolved temperatures. Finally, possible mechanisms that may be contributing to the temperature anomaly distribution in the Late Maunder Minimum are discussed in view of the model results. The paper is closed by the conclusions.

2 Model description and experiment

The global climate model consists of the spectral atmospheric model ECHAM4 (Roeckner et al., 1996) and the ocean model HOPE-G (Wolf et al., 1997), both developed at the Max-Planck-Institute of Meteorology in Hamburg. The model ECHAM4 has in this simulation a horizontal resolution of T30 (aprox. 3.75°x 3.75°) and 19 vertical levels, five of them located above 200 mb. The horizontal resolution of the ocean model HOPE-G is about 2.8°x 2.8 ° with a grid refinement in the tropical regions, where the meridional grid-point separation decreases progressively to the equator, reaching a value of 0.5°. This increased resolution allows for instance for a more realistic

representation of ENSO events. The ocean model has 20 vertical levels.

To avoid climate drift in such a long simulation, additional fluxes of heat and freshwater are applied to the ocean. These fluxes were diagnosed in a coupled spin-up integration with restoring terms that drive the sea-surface-temperature and sea-surface salinity to their climatological observed values. This flux adjustment is constant in time and their global integral vanishes.

Two simulations with this model have been carried out. In a control simulation the external forcing was kept constant in time and set to the values of the present climate. The model was integrated for 1000 years. In the second simulation the coupled model ECHO-G was driven by estimations of three past external forcing factors: solar variability, greenhouse gas concentrations in the atmosphere and an estimation of the radiative effects of stratospheric volcanic aerosols, in the period 1550-1990 A.D.. No changes in the anthropogenic atmospheric aerosol concentrations have been considered.

The atmospheric concentrations of two greenhouse gases, carbon dioxide and methane, have been estimated from analysis of air bubbles trapped in Antarctica ice cores (Etheridge et al., 1996; Blunier et al.,1995). The past variations of solar output have been derived from the values used by Crowley (2000). In the period after 1610 A.D., past solar variations are empirically estimated from observations of sun spots (Lean et al., 1995) and between 1500 and 1610 A.D. they are based on concentrations of the cosmogenic isotope ^{10}Be. Crowley (2000) used these values to drive an energy-balance climate model, i.e. the represent the external net input of short-wave radiation to the climate system. To represent these variations in the ECHO-G simulations these values have been translated to variations in the solar constant, with no optical wavelength discrimination.

The third external factor is the effect of volcanic aerosols. The estimation of this factor is arguably loaded with the largest uncertainties. Some indices exist that, to some extent, try to reflect the variations of transparency of the stratosphere due volcanic eruptions, the Dust Veil Index or the Volcanic Explosivity Index. They are based on important characteristic of known past volcanic eruptions, such as location, season and mechanical energy liberated in the eruption. Also, information from known short-term climate changes after the eruption may be taken into account in the elaboration of the index, which to some extent hinders their use as external forcing in a climate simulation, since they are not completely independent of the effects that one is trying to simulate (Briffa et al., 1998). Probably, more accurate for the purposes of a climate model simulation are derivations of past optical depths of the stratosphere based on

acidity measurements in ice cores. From the climatic point of view one of the most important effects of volcanic eruptions is conveyed by acid gases liberated in the eruptions. They are then oxidized into aerosols form in the atmosphere to sulfuric acid. In the troposphere the acid aerosols are washed out by precipitation, which eventually modifies acidity of the ice formed at the ice-core location. Optical densities of the stratosphere can be thus estimated from ice acidity through a semi-empirical model. One important advantage of this approach is the availability of long continuous time series of average atmospheric optical density. However, the ice acidity is also influenced by other factors that are not directly related to the volcanic eruptions, such as atmospheric transports, precipitation or dry deposition. Furthermore, potentially important information cannot be retrieved from these measurements. For instance, the timing and location of the eruption or the time elapsed between eruption and ice deposition are very difficult to estimate if the eruption is unknown from other sources. In view if this uncertainty one can only hope to be able to include in the climate simulations the most coarse effects of volcanic eruptions, for instance the very large eruptions or the accumulation, or absence, of volcanic eruptions in certain periods of time. We stick therefore to the same dataset used by Crowley (2000) in his energy-balance climate simulation. These are global annual estimations of atmospheric optical depth translated to short-wave radiative forcing. As in the case of the solar variability we translate his numbers to effective variations of the solar constant used in the ECHO-G simulation. It should be noted that this a globally and annually averaged estimation of the effects of volcanic eruption on the radiative balance of the Earth. Thereby the, potentially important, regional and timing details of the eruptions are not communicated to the climate model. Fig.1 shows the time evolution of these forcing factors as used in forced climate simulation. Perhaps, a more realistic approach that could be pursued in future simulations is the prognostic simulation of the aerosols distribution in the stratosphere and high troposphere. However, for this purpose the climate model should include a realistic model of the stratosphere with enough vertical resolution- something which the present version of ECHO-G does not. Furthermore, standard initial distributions of volcanic aerosols should be prescribed depending on the location and intensity of the eruptions and on the chemical composition of the erupted gases.

Since this simulation was initiated, another estimation of stratospheric optical depth in the last centuries with latitudinal resolution, has become available (Robertson et al., 2001). As illustration of the uncertainties included in these estimations Figure 2 shows a comparison of the time series of volcanic radiative forcing from Robertson et al. (2001), translated in the same way

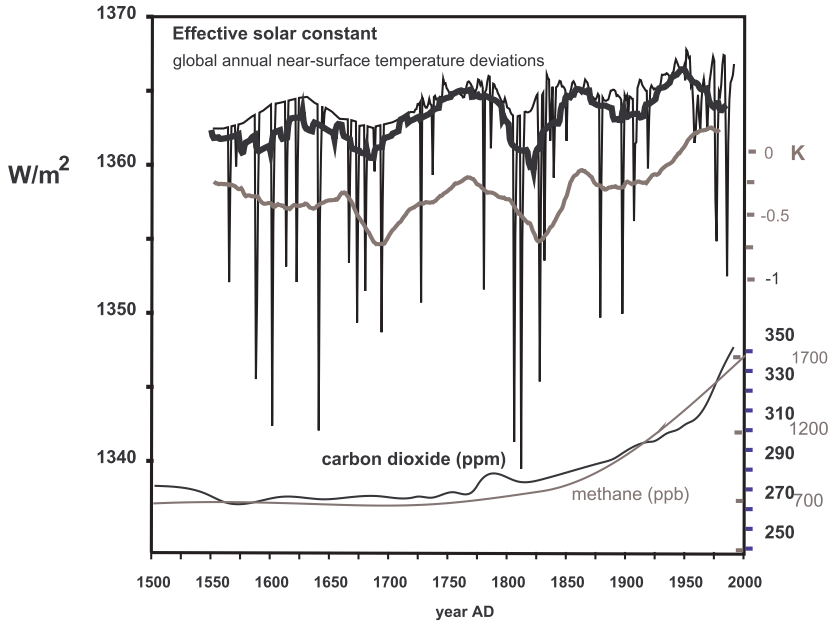

Figure 1: Effective solar constant (solar forcing plus effect of volcanic aerosols; thick red line is a 26-year running mean), concentrations of carbon dioxide and methane used to drive the climate model, and the simulated annual global near-surface temperature, filtered with a 26-year running mean.

as the Crowley (2000) forcing data to effective variations of the solar constant, and subsequently globally averaged. Both curves show great similarities in the timing of large eruptions and in the periods where eruptions happened more frequently. However, for some individual eruptions the disagreement between both estimations can be of the order of 50%.

3 Evolution of the near-surface air temperature

The simulated global near-surface temperature in the forced model integration exhibits a larger variability than the control run (Fig 1). Two clear minima, at the end of the 17^{th} century and beginning of the 19^{th} century, are simulated. These minima occur almost simultaneously (after a 2-3 year lag) with known minima in the solar activity, the Late Maunder Minimum and the Dalton Minimum, respectively.

Paleoclimatic temperature reconstructions have not targeted the same variable (global, hemispheric, annual or seasonal temperature), so that their comparison is not straightforward (Briffa and Osborn, 2002). One strategy so far has been to re-scale the different reconstructions to a common framework using scaling factors derived from the instrumental record in the 20th cen-

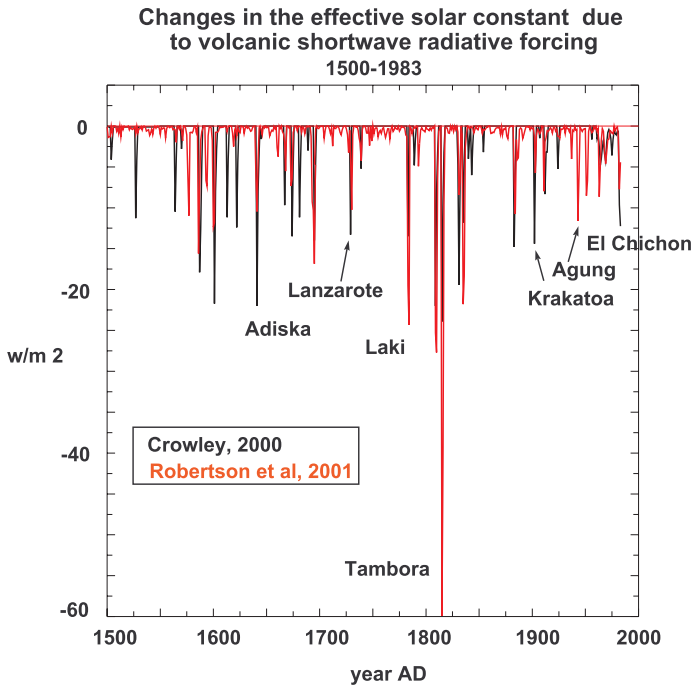

Figure 2: Variations in the effective solar constant due to volcanic aerosols derived from estimations of the radiative aerosol forcing from Crowley (2000) and Robertson et al. (2001). The original, latitudinally resolved, optical density data from Robertson et al. (2001) have been globally averaged and translated to radiative forcing in the same way as in Crowley (2000).

tury, thereby assuming that the proportionality factors are also valid for temperature variations at centennial timescales. To avoid these uncertainties in the re-scaling, figure 3 shows several original (not re-scaled) Northern Hemisphere temperature reconstructions, together with the annual temperature in the whole Northern Hemisphere and summer temperature in the northern extratropical regions simulated by the ECHO-G model.

The simulated degree of cooling along the last centuries, about 0.6-0.7 K relative to the 1900-1990 mean, agrees reasonably well with the extratropical dendrochronological reconstruction of ECS and with the bore-hole estimations (Huang et al., 2000), both being the ones indicating coldest conditions in the LIA. In particular, the agreement with ECS around the Dalton Minimum and the temperature trend in the last 200 years is remarkable. However, the agreement of the ECS reconstruction and the model in the LMM is not perfect. The ECS curve indicates colder conditions around 1600 A.D. than in the LMM, in contradiction with other proxy evidence and the JBBT reconstruction. It should be pointed out that the ECS reconstruction

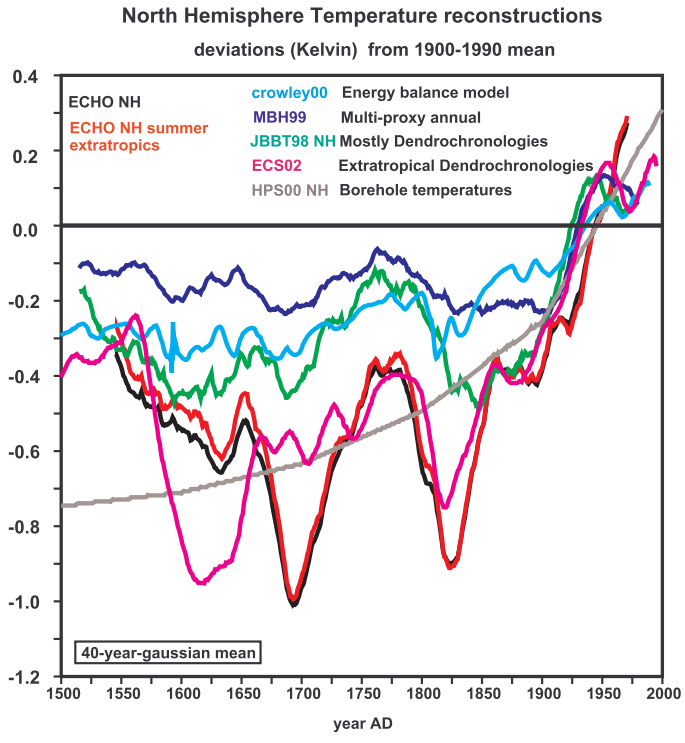

Figure 3: Time series of annual Northern Hemisphere and summer northern extratropics mean temperature anomalies (deviations from 1900-1990 mean) simulated by the climate model ECHO-G, compared to a simulation with an energy balance model (Crowley, 2000), and with reconstructions of Northern Hemisphere mean temperature based on a multiproxy dataset (MBH99), only dendrochronological data (ECS02), various normalized paleo-data of various types records (JBBT98), and on borehole measurements (HPS00). Time series have been smoothed to represent frequencies lower than 40 years. Note that the individual reconstructions have not been rescaled to represent a common season.

is expected to contain little useful information at periods shorter than 20 years (Esper et al., 2002) and the duration of the LMM in the model is close to this limit. From the model point of view, the other reconstructions and the energy-balance-model simulation of Crowley (2000) seem to underestimate the degree of cooling. For instance, when the uncertainty of the MBH99 reconstruction, in terms of two standard error confidence is taken into account (not shown), the model reconstruction is consistent with the MBH99 estimate before and after the LMM. During the LMM (and the Dalton-Minimum around 1810 A.D.), however, the climate model is suggesting values clearly different from MBH99 reconstruction.

The much larger variability at the very-long time scale in the model may have several origins:

a too large sensitivity of the model against variations in the external forcing, biases in the external forcing itself, or an underestimation of the temperature changes by the empirical climate reconstructions. As stated before, the estimation of the global atmospheric optical density based on the Greenland ice-cores acidity may contain large errors and this might be partially a source for the large LIA and LMM cooling simulated by the model. To ascertain this point, further simulations with other estimations of the volcanic radiative forcing would be necessary. The sensitivity of the model can be estimated, at shorter timescales, by comparing the centennial trends in the instrumental period with the available instrumental temperature records. Figure 4 shows the Northern Hemisphere annual temperatures simulated by the ECHO-G model and derived from the instrumental dataset by Jones et al. (1999). For this comparison the ECHO-G data have been decimated to the grid-points that are covered in the Jones et al. (1999) instrumental dataset. In the analysis of MBH99 the statistical reconstruction was calibrated against this instrumental dataset and therefore they automatically represent the spatially decimated average temperature. Figure 4 shows that the model simulations tend to be already too cool in the last 150 simulation years. The linear trends calculated from 1856 onwards support this impression: 0.48 K, 0.66 K, 0.30 K and 0.47 K per century for the instrumental data, ECHO-G, MBH99 reconstructions, and the JBBT98 reconstructions, respectively. However, the interannual standard deviation calculated in the same period after linearly detrending the series indicates that the interannual variability of the model is in line with the observations, whereas the statistical paleoclimatic reconstructions are both somewhat less variable (0.21 K,0.21 K, 0.12 K and 0.18 K, respectively). It seems, therefore, that the model may be somewhat overestimating the long-term trends caused by variations in the external forcing. This overestimation seems, however, not very severe, but it should be put in the perspective of future climate simulations with other models. The model ECHO-G has also been used to simulate the climate of the next decades under a scenario of 1% annual increase in the atmospheric CO_2 concentrations, similar to the IPCC IS92a scenario. The level of near-surface warming from today's level simulated by this model lies roughly in the middle of the range of the IPCC simulations, namely 1.70 K at doubling of the present CO_2 concentrations and 3.45 K in year 2100 A.D..

The low-frequency temperature variations in the model are not symmetrically distributed in the Northern and Southern Hemisphere, although the model is driven by hemispherically symmetric external forcing. Figure 5 reveals the hemispherically average air temperature in the summer season for the southern hemisphere. The centennial variability is clearly lower in the

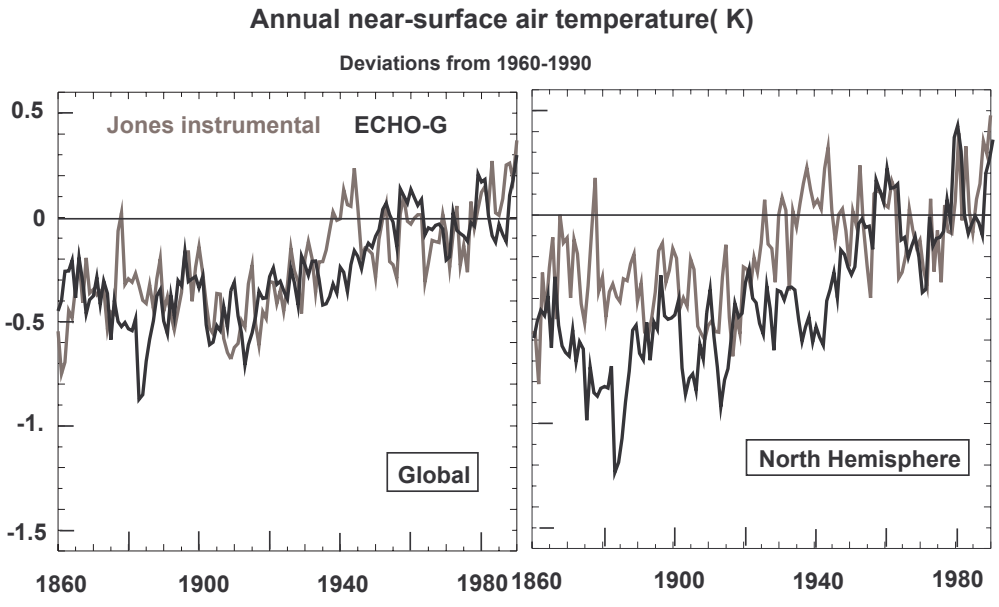

Figure 4: Mean annual near-surface air temperature deviations simulated by the ECHO-G model and derived from the instrumental record (Jones et al, 1999)). The model output has been decimated to match the grid points covered in the observational dataset.

Southern Hemisphere than in the Northern hemisphere, both in the JBBT98 reconstruction and in the ECHO-G simulation, quite probably due to the damping effect of the ocean masses. But, as in the Northern Hemisphere, the model tends to simulate colder conditions through the LIA than in the reconstructions. In particular, although the timing of the Maunder Minimum and Dalton minimum agrees, the magnitude of the temperature deviations is about twice as large in the model. Also, a clear lag around 1900 A.D. is observed between model and reconstruction. However, the temperature trends since 1900 A.D. until 1990 agree remarkably well.

4 North Atlantic Oscillation

We turn our attention to one the most important atmospheric circulation patterns in the extratropics in winter time, the North Atlantic Oscillation (NAO). Usually the spatial patterns of this mode is defined as the leading EOF of the sea-level-pressure field in North Atlantic-European sector. The corresponding patterns calculated from the climate simulation in the period 1900-1990 A.D. is shown in Figure 6. This pattern describes the intensity of the low-level westerly winds at midlatitudes and compare quite well with their counterparts obtained from observational datasets (Hastenrath and Greischar, 2001). Also their fingerprints on the temperature and precipitation fields agree well with observations (Zorita and González-Rouco, 2002). Some

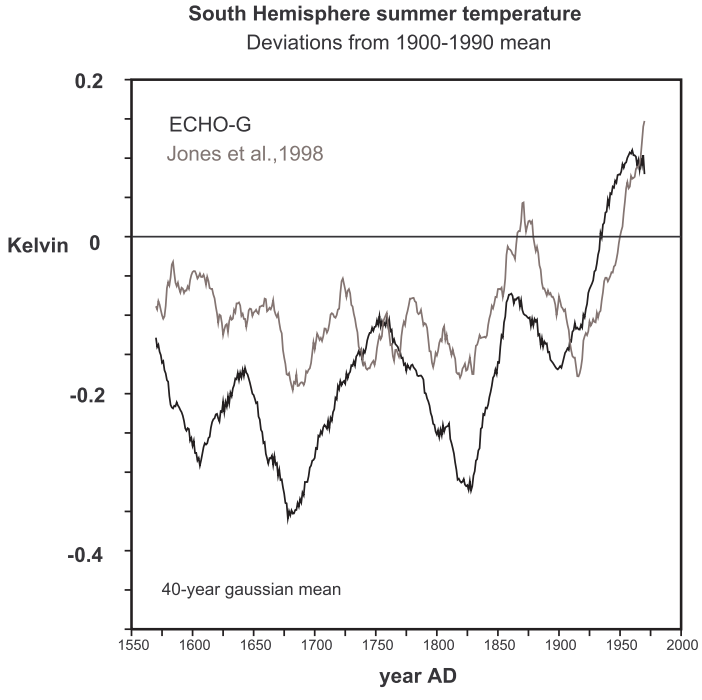

Figure 5: Time series of Southern hemisphere summer air temperatur e anomalies (deviations from 1900-1990 mean) simulated by the climate model ECHO-G, compared to the dendrochronological reconstructions by JBBT98

differences with the observations are, however, also evident, for instance, the stronger intensity of the North Pacific Center of action of the Arctic Oscillation in the model and a shift of the both center of action of the NAO towards the Eurasian continent.

The atmospheric circulation presents a high degree of internal variability at high frequencies, and the effect of external forcing on the atmospheric indices is expected to be small. For instance, SLP is one of the variables where the signal-to-noise ratio in climate change simulations is smallest. Therefore only a rough agreement between the evolution of the simulated atmospheric indices and the empirical reconstructions can be expected. Furthermore, there exist several empirical reconstructions of the NAO index which disagree with one another (Schmutz et al., 2000). Figure 6 shows the simulated NAO index, calculated as the principal component of the first EOF of the simulated DJF SLP field in the North Atlantic sector, together with two recent empirical reconstruction (Luterbacher et al, 2002b; Cook et al., 2002; Glueck and Stockton, 2001). These four indices disagree in several aspects, but they roughly agree in the maximum reached around 1725 A.D. and the subsequent evolution towards lower values of the NAO until

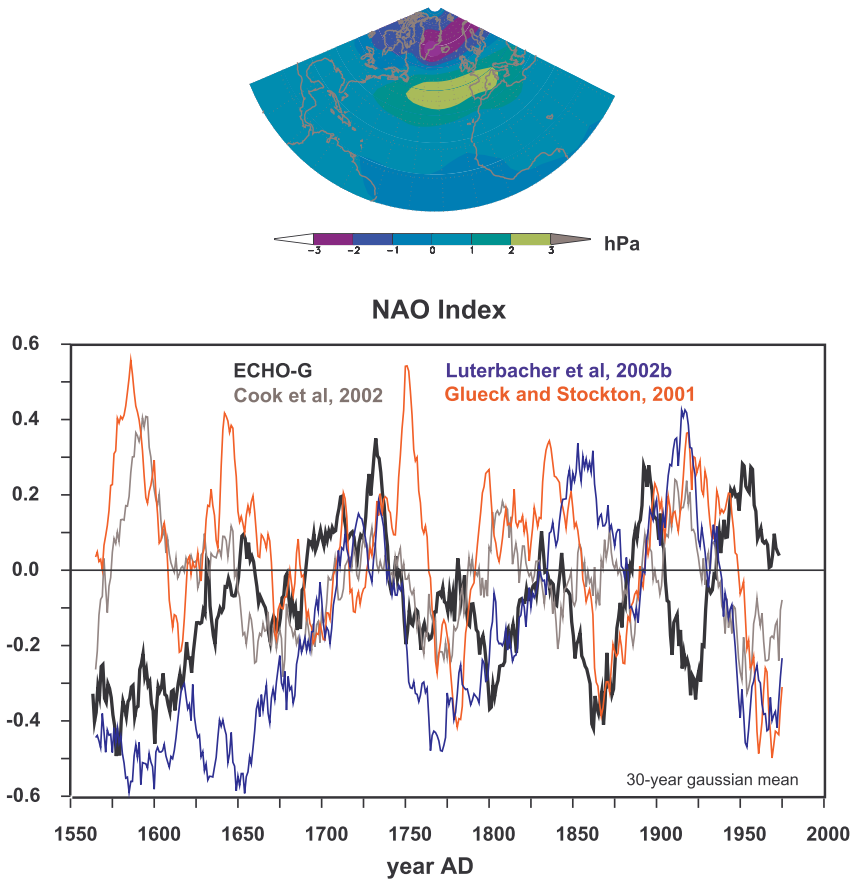

Figure 6: Patterns of the North Atlantic Oscillation as result of an EOF analysis of the simulated SLP fields in winter time in the period 1900-1990 in the North Atlantic-European sector, and the North Atlantic oscillation index, simulated by the model ECHO-G and reconstructed by several authors. The annual indices have been standardized to unit variance and to zero mean in the period 1900-1990

1750 A.D.. Noteworthy is the strong positive trend of all NAO indices throughout the LMM, roughly from 1650 A.D. until 1725 A.D., in contrast to the equilibrium simulation by Shindell et al. (2001), where the index remains in a quasi-permanent low index phase during the LMM. From 1750 A.D. onwards the Luterbacher et al. and Glueck and Stockton (2001) reconstructions indicate an evolution to higher NAOI values. Around 1875 A.D. all NAO indices, with the exception of Luterbacher's et al., reach a minimum. From there on, all empirical reconstruction show subsequently roughly the same behavior as they both have been fitted in the instrumental period, whereas the simulated NAO index evolves clearly at variance with the empirical reconstructions. The question of the relative amount of variance that is related to internal variability and to external forcing can only be ascertain with ensemble simulations. Giorgi and Franciso

(2000) have found that the simulated changes in the NAOI in climate change experiments may strongly depend on the internal model variability. It can be reasonably expected that the signal of the external forcing on the atmospheric circulation is only visible in periods with high deviations of the external forcing, e.g. the Late Maunder Minimum, the Dalton Minimum and the last decades of the 20 th century. The NAOI reconstructions themselves have also been a matter of concern, since the disagreement among them is too apparent (Schmutz et al., 1999). For instance, although the correlation between the most recent NAOI reconstructions (Cook et al., 2002; Luterbacher et al., 2002b) is relatively high (~ 0.5) at interannual timescales, even in some periods far away from the calibration period, their coherence at decadal timescales breaks down (Figure 6). A possible explanation for this behavior may lie in the different information contained in temperature and precipitation proxies at long timescales (Zorita and González-Rouco, 2002), inspite of the relatively high correlation of the different proxies at interannual timescales.

The comparison of the model NAOI with the empirical reconstructions requires a relatively strong low-pass filter to enhance the possible effect of the radiative forcing on the atmospheric circulation relative to the strong interannual variability. However, this low-pass filter masks the behavior of the NAO within the two temperature minima, the LMM and the Dalton minimum. This behaviour is described in more detailed in the following section.

5 The Late Maunder Minimum

We turn now our attention to the winter (December-February) air temperature in the decades 1675-1710, where the model simulates an intense global cooling, coincidental with the Late Maunder Minimum found in most European proxy indicators (e.g. Luterbacher et al., 2001). The Late Maunder Minimum was a period at the end of the 17th century of diminished solar irradiance, with several large volcanic eruptions (Briffa et al., 1998). It is thought to mark the coolest phase of the Little Ice Age. In the model simulation a marked minimum of the globally averaged near-surface air temperature occurs around 1690 A.D., which is in agreement with the findings of Mann et al. (1999) and Luterbacher et al. (2003, personal communication) for Europe. In the following a more detailed analysis of the 30 years around this minimum, 1680-1710 A.D., is presented. Recently, spatially resolved empirical temperature reconstructions for the European region covering this period have been achieved (Luterbacher et al., 2003, personal communication) and this reconstruction is compared with the output of the climate model. In

the analysis of the LMM the long-term mean in the period 1550-1850 A.D. is take as reference mean state to avoid the signal due to anthropogenic greenhouse warming.

5.1 Simulated and reconstructed European temperature

A broad spectrum of early instrumental station temperature and pressure series from London and Paris (Mannley, 1974; Legrand and Legoff, 1992; Slonosky et al., 2001) as well as several indexed temperature and precipitation from various sites are available for the LMM (Wanner et al. , 1995, Pfister,1999; Raez et al., 1999; Alcoforado et el., 2000; Barriendos, 1997; Xoplaki et al., 2001; Luterbacher et al, 2001 Glaser, 2001). The latter are derived from documentary evidence and/or from natural archives (narratives, annals, scientific writings, monastery records, direction of cloud movement, wind direction, warm and cold spells, freezing of water bodies, droughts, floods, and information on vegetation). Together with the sea ice conditions off the coasts of Iceland (Ogilvie, 1996) and the ice winter severity in the Western Baltic (Koslowski and Glaser, 1999) a total of around 20 winter climate time series covering the areas of north-western, central, eastern and southern Europe are available for the assessment of the LMM. These time series have been used to statistically reconstruct large-scale, gridded (0.5° lat. x 0.5° lon.) land based winter temperature fields for the LMM for the European land areas (30W to 40E; 30N to 70N). The statistical method is based on an Empirical Orthogonal Function (EOF) analysis of the predictor field (the proxy climate indicators) and of the predictand field (the gridded instrumental air temperature). Standard statistical regression models linking both sets of Principal Components are setup. The statistical equations are calibrated in the period 1901-1960 and validated in 1961-1990. In the validation, the strength of the linear statistical relationship between reconstruction and observation is measured by the Reduction of Error (RE) in each grid point. This is a measure of the quality of the reconstruction between $-\infty$ and 1 (the case for a perfect reconstruction). Positive values of the RE indicate some skill in the reconstruction. After assessment, the statistical parameters were recalibrated in the period 1901-1990 in order to derive seasonal winter temperature fields for the LMM. For a detailed mathematical treatment of the reconstruction method, the reader is referred to Luterbacher et al. (2002ab).

It is believed that 50-80% of the real variance is recovered by the reconstruction. Over Iceland and north-eastern Europe including Russia, the skill is only 20 to 30%, so that there

should be some reservation with the reconstruction here. For instance, only sparse information is available for winter conditions in Finland. Some extremely cold winters are mentioned in the historical records, but for many winters it is not known whether they were warmer or cooler than normal (Luterbacher et al., 2003, personal communication)

Figure 7a shows the reconstructed temperature departures from the 1550-1800 mean, together with the estimated RE. Cooling during the LMM was widespread in Europe, with departures of more than 1.2K in Eastern Europe and Western Russia, up to 1 K in Central and Western Europe and up to 0.5K over the Mediterranean, the British Isles and parts of Scandinavia. Up to 0.5K higher temperatures were reconstructed only over SE Greenland, Iceland and parts of western Scandinavia. There is evidence of worsening climatic conditions in the Russian North starting at the beginning of the LMM however the degree of cooling is not given (Borisenkov, 1994). Warming was estimated to have taken place only in a few locations in northern Norway, Iceland and southeastern Greenland. The confidence in these estimates is low in areas with little historical evidence, in particular Finland, Russia and in the alleged warmer-than-normal spots. According to the RE values, the estimate is representative over Western and Central Europe, South-western Scandinavia, the Balkan and most of the Mediterranean area, while the RE values are rather small over most of Russia, Northern Scandinavia, Iceland and Greenland. Another benchmark for the reconstruction quality is consistency with independent data that was not used in the temperature reconstruction, for instance, Eastern Europe (Bohemia and Moravia, Bradzil et al., 1994), and the The Netherlands, Belgium and Luxembourg (van Engelen et al., 2001).

The reconstruction compares well with the modeling result (Fig. 7b), which shows a cooling almost everywhere, with maximum values of 1.2K and more in Eastern Europe, and 0.5K and more over most of Europe. According to a local t-test, the cooling is systematic, and not due to random variations, almost everywhere in Europe, Iceland and southern Greenland, with the exception of North-western Norway. Taking into account the local significance in Figure 7b and the RE-values for Figure 7a, the two diagrams appear as remarkably consistent, both indicating an enhanced continentality in Europe during the LMM relative to the long term mean.

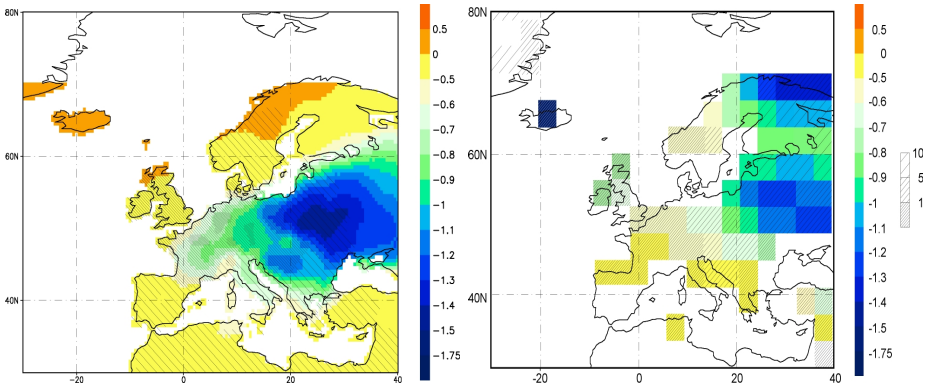

Figure 7: Winter (DJF) mean temperature differences 1675-1710 minus 1550-1800 in Europe according to early instrumental and documentary evidence (a) and model (b). In (a) the statistical model performance (RE) for the LMM winter temperature reconstructions is given by hatching (dense > 0.9, medium > 0.7 and light > 0.4). In (b) the statistical significance, as obtained by testing the local null hypothesis of equal means, is indicated by hatching: dense $< 1\%$, medium $< 5\%$ and light $< 10\%$.

5.2 Regional Circulation Anomalies and European Climate

To analyze the influence of the atmospheric circulation changes on European temperature anomalies the NAO index has been determined as the difference between the area averaged and normalized mean sea-level pressure anomalies representing the teleconnectivity centers located Northwest of Portugal and over Iceland as in Ulbrich and Christoph (1999). In Fig. 8 the modeled annual European mean 2m temperature has been displayed in relation to the modeled NAO index for the time period 1550-1850. During approximately the initial period of the LMM (1671-1684) the NAO index is negative, together with a sharp drop in temperature, indicating that advection of continental cold air dominates in central Europe. This can be confirmed by a significant decrease of storm track activity (defined as the 2.5 to 6 day band pass filtered variance of the 500 hPa geopotential height) in the North Atlantic and West European region (Fig. 9). The NAO then turns positive approximately in the second half of the LMM (1685-1708) with European warming simultaneously. The enhanced advection of warmer Atlantic air masses contributes to the decay of the LMM, approved by an significant increase of storm-track activity over the European continent (Fig. 9). This cooling-warming transition can also be verified with the temperature reconstruction of van den Dool et al. (1978). For the Dalton Minimum at the beginning of the 19^{th} century, which is also part of the simulation, a similar behaviour can be seen.

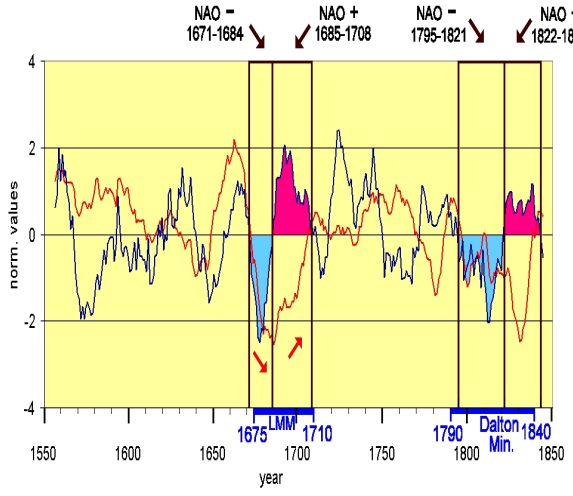

Figure 8: Modeled European annual mean temperature (red curve) and NAO index (blue curve) for the time period 1550-1850 (11 year moving average). In the period (1671-1684, cooling phase) the NAO index is negative, in the period (1685-1708, warming phase) the NAO index is positive. The Dalton Minimum shows a similar feature.

5.3 Global climate anomalies in the Late Maunder Minimum

The simulated near-surface temperature anomaly distribution during the LMM is displayed in Figure 10a. In Northeast Canada, Greenland and the northern North Atlantic a strong cooling

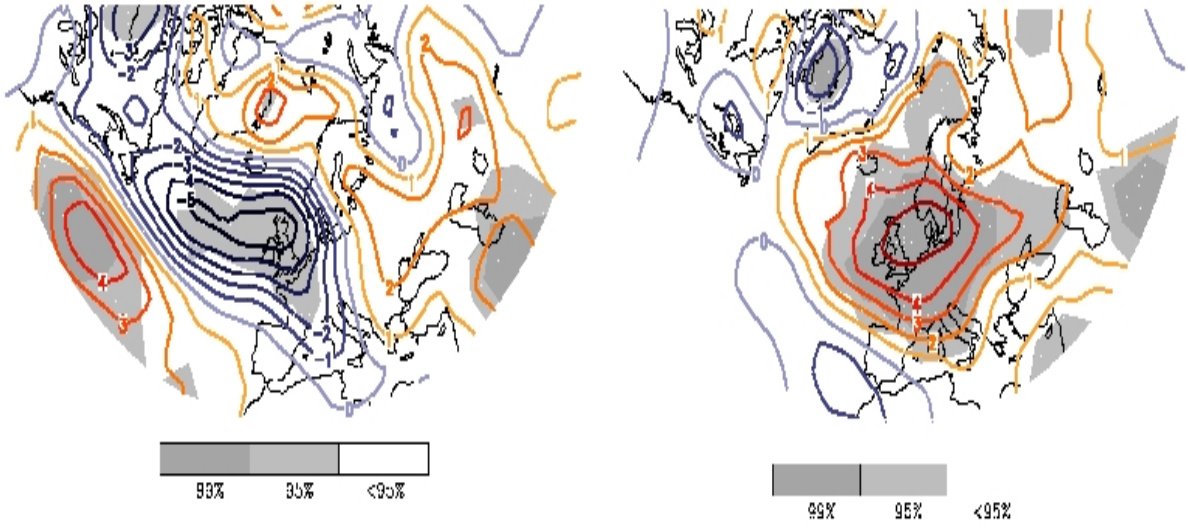

Figure 9: Difference of storm track activity, defined as the 2.5 to 6 day band pass filtered variance of the 500 hPa geopotential height [units: gpm], for the (1671-1684) period (left) and (1685-1708) period (right) relative to a reference period (1551-1800 except LMM). They grey areas indicate the significance in percent according to a Student t-test.

of the order of 1K and more is evident. Over the NH continents a weaker cooling, of 0.5K and more, is prevalent. Over most of the rest of the globe a cooling of up to 0.5K is simulated, with isolated regions of warming in the Southern Hemisphere. This signal is statistically significant according to a local t-test, for the area north of about 30S (not shown). Thus, the simulated event is a worldwide phenomenon, which is associated with the largest anomalies in the North Atlantic. The overall cooling is consistent with evidence from tropical coral proxy data (Quinn et al., 1998;) and the findings for North America (Fritts and Lough, 1985; Dunbar and Cole, 1993), China (Wang et al., 2001; Yang et al., 2002; Ge et al., 2003), South Africa (Holmgren et al., 1999) and Southern America (Villalba et al., 2002).

The air temperature anomaly distribution can be also found almost unchanged in the middle troposphere at 500 mb height (Fig. 10b), but a qualitative deviation from this spatial structure is observed at 200 mb ((Fig. 10c), where the polar regions actually show positive temperature anomalies with respect to the long-term mean. This behavior has been previously described by Shindell et al (2001) in an equilibrium experiment with an atmospheric model coupled a mixed layer ocean, forced by LMM solar irradiance. This will be discussed in the next subsection.

In the Labrador Sea and the North Atlantic South of Greenland ice conditions are much more severe than before and after the LMM event, with the ice coverage increased by up to 25% (Fig. 11a). This increased ice cover is probably the reason for the greatly diminished near-surface air temperature south of Greenland. The simulated sea-surface temperature anomalies are depicted in Fig. 11b. The North Atlantic, and to a lesser extent the North Pacific, display cooler temperatures than the rest of the ocean surface, which is in general also colder than the long-term mean. An exception is found in the Southern Oceans, where the SST anomalies are slightly positive. This SST anomaly distribution constitutes therefore a dipole between the Northern and Southern Ocean at middle and high latitudes. Similar dipole patterns have been derived from paleotemperature reconstructions from proxy data, albeit at much longer timescales, and are thought to be a result of variations in the global thermohaline circulation (Stocker, 2002). Salinity at 100 m depth is lower than the long-term mean in the North Atlantic with clear positive anomalies in the Tropical Atlantic and North Pacific (Fig. 11c). The ice cover and salinity anomalies in the North Atlantic are reminiscent of the Great Salinity Anomaly (GSA) observed in the North Atlantic in the late 1960's and 1970's. According to Mysak et al. (1990) hypothesis the ice cover associated to the GSA could have its origin in an excess of freshwater input into the North Atlantic through increased precipitation minus evaporation in the North

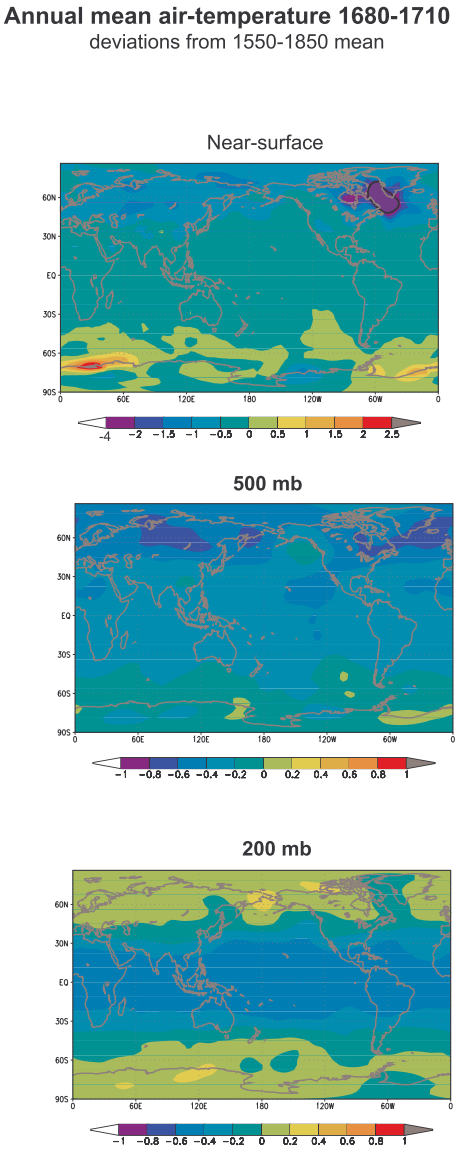

Figure 10: Climate anomalies in the LMM relative to the long-term mean 1550-1850 A.D.: a) annual near-surface air temperature;b) air-temperature 500 mb; c) air-temperature 200 mb.

Atlantic-Labrador Sea sector. The fresher water masses would freeze more easily. The ice produced in this way could be then advected to regions where ocean convection takes place, thereby affecting the deep water production. Other mechanisms have been proposed to explain extreme GSA and ice cover events simulated in coupled climate models (Hall and Stouffer, 2001). In their simulation, anomalously strong and persistent northerly winds cause an increased ice export from the Arctic Ocean that subsequently melts and freshens the North Atlantic waters.

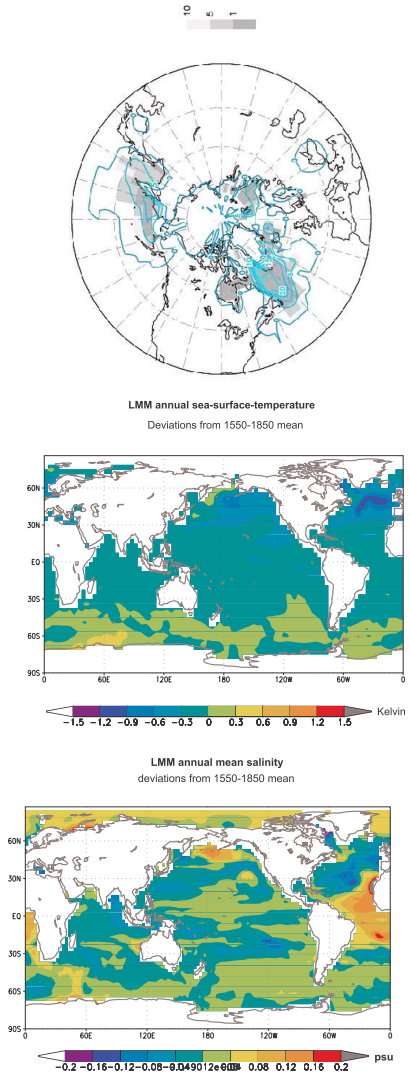

Figure 11: Climate anomalies in the LMM relative to the long-term mean 1550-1850 A.D. : a) sea-ice coverage (percent, gray scale shows significant differences at the 1%, 5% and 10% significance level.); b) sea-surface temperature; c) salinity at 100 m depth

The large salinity anomalies at 100 m depth in the Tropical Atlantic are restricted to the upper ocean layers and are not visible at 450 m depth. They are not related to clear freshwater fluxes at the surface nor to horizontal advection by ocean currents, so that they are probably associated to a deepening of the thermocline in the Eastern Tropical Atlantic.

5.4 Physical mechanisms involved in the Late Maunder Minimum

In the decades surrounding the LMM the near-surface temperatures are almost everywhere lower than the long term mean, in accordance with the reduced solar irradiance and increased volcanic activity. The ECHO-G model responds to the reduced equivalent solar forcing clearly more strongly than the energy balance model of Crowley (2000), which simulates a much more moderate temperature reduction. This holds even if the North Atlantic sector at high latitudes is left out when calculating the global mean temperature change. The simulated temperature change approaches the estimation of the energy-balance model of Crowley only when the high latitudes are excluded to calculate the global mean. This suggests that the sensitivity of the ECHO-G model is considerably stronger than the one assumed in the parametrization in the energy balance model of Crowley (2000), probably because of feedback processes at high latitudes that are not captured in the energy-balance model. In climate simulations with a 1% annual increase of atmospheric greenhouse gases, the sensitivity of the ECHO-G model lies roughly in the middle of the range of the IPCC simulations, namely 1.70 K at the doubling of the present CO_2 concentrations and 3.45 K in year 2100 A.D.. The sensitivity of the ECHO-G model to changes in the radiative forcing is therefore in line with that of other rmodels.

The global distribution of SST or near-surface temperature anomalies during the LMM is, apart from the positive anomalies in the Southern Hemisphere, compatible with the weaker solar insolation and stronger volcanic activity. At high latitudes in the northernocean basins the temperature drop is higher that average, specially in the North Atlantic off South Greenland. The SST anomaly distribution is indicative of a change in the strength of the Western Boundary Current systems, the Golf Stream and the Kuroshio as shown in the intensity of the mean annual stream function at 100 meter depth (Figure 12). The spatial stream function patterns describe in both basins the strength of the gyre circulation. Both stream indicators show that in the LMM these current systems were weaker than in the long-term mean and that they are also coupled in time to the annually averaged global temperature and therefore to the effective radiative forcing. This also can explain why the intensity of both current systems evolves in phase in this period. Figure 12 also shows, as a measure of the average atmospheric forcing on the ocean surface, the annually averaged wind-stress curl, spatially averaged over the ocean grid-points in each basin (the basin integral of the ratio of the wind stress over the Coriolis parameter yields a similar picture). It is evident that the current indicators evolve as a response

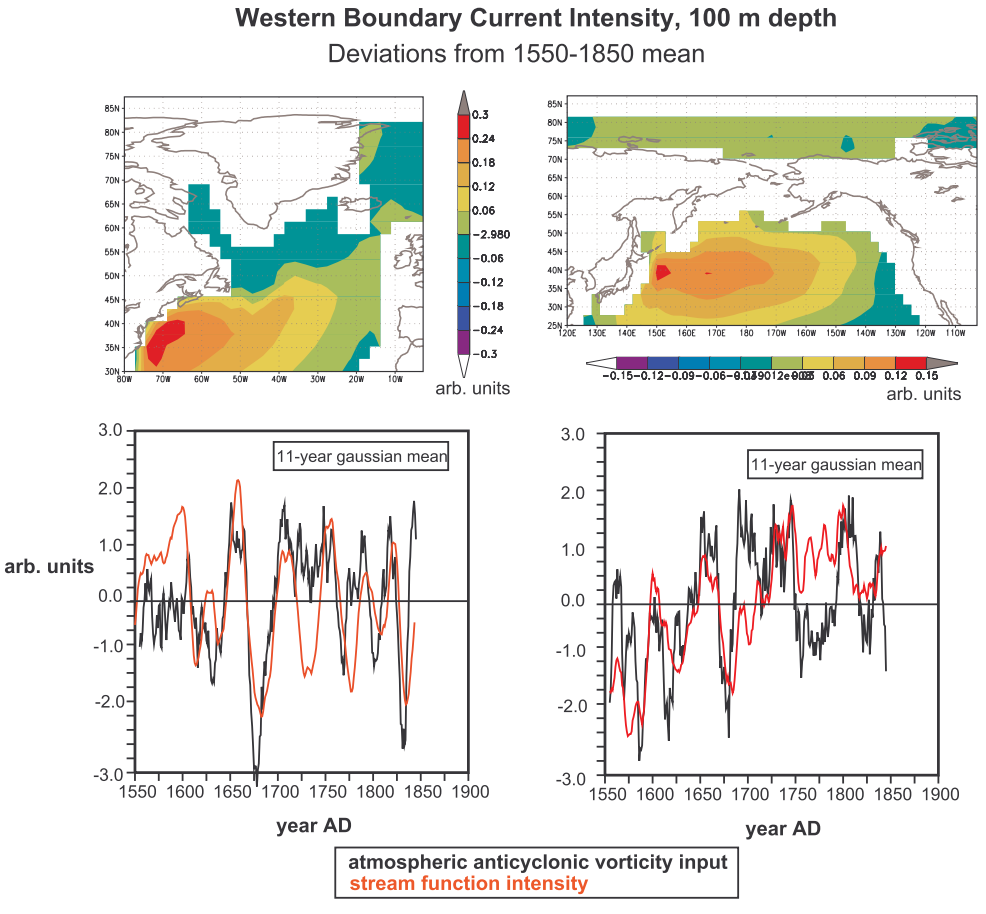

Figure 12: Mean annual stream function at 100 m depth in the North Atlantic and North Pacific (positive, anticyclonic circulation), together with their intensity evolution in the period 1550-1850 A.D. and the annual wind stress vorticity (positive, anticyclonic) averaged over the ocean-gridpoints in the respective ocean basins. Anomalies are relative to the long-term mean 1550-1850 A.D..

to the atmospheric vorticity input, which at these timescales and at basin-wide spatial scales also evolve in phase. To first order, apart from the globally reduced solar input that causes an almost global cooling, the explanation for the simulated near-surface temperature anomalies in the LMM at high latitudes would involve the weakening of the Western Boundary systems as a response of the atmospheric circulation.

The atmospheric circulation would then have changed as a response to changes in the radiative forcing. The influence of changes in the radiative forcing onto the atmospheric circulation has not been completely established yet. In general, scenario simulations for the next century (increasing radiative forcing) tend to indicate a strengthening of the atmospheric zonal indices

(Shindell et al.,1999; Fyfe et al., 1999; Zorita and González-Rouco, 2000). At shorter timescales, the LMM (decreased radiative forcing) simulations by Shindell et al. (2001) show a weakening of the NAO index. In the present simulation, with an interactive three-dimensional ocean, this is reflected in a reduced anticyclonic vorticity input to the ocean surface in the subtropical gyres, slowing the western boundaries currents and thereby intensifying the temperature drop at middle and high latitudes in the Northern Ocean basin.

The connection between the equator-to-pole temperature gradient at 200 mb and the anticyclonic vorticity input is illustrated in figure 13. The temperature gradient evolves very nearly in phase with the wind-stress forcing before and during the LMM, although the agreement is not so good in later decades in the simulation, specially during the Dalton Minimum (not shown). According to the results of Shindell et al. (2001), an increased solar insolation should cause a stronger warming of the Tropical higher troposphere than in the lower polar stratosphere, thereby intensifying the zonal wind in the lower stratosphere. This enhanced zonal wind would be able to reflect equatorwards more effectively the vertically propagating gravity waves from the lower troposphere, intensifying the northward momentum flux in the troposphere, i.e. leading to a stronger zonal index. This higher wave reflectivity at the tropopause hinders also the vertical heat transport by waves into the stratosphere. The situation with reduced solar insolation should be the one reversed. The ECHO-G model, however, lacks a realistic representation of the stratosphere, both dynamical and chemical, and it is therefore surprising that this mechanism could be also responsible for the reduced temperature gradient at 200 mb in the present simulation. But otherwise, the positive temperature anomalies at 200 mb in the polar regions (Fig. 10c) are difficult to reconcile with the reduced solar insolation in the LMM. When the pattern of LMM simultaneous temperature anomalies (near-surface and at 200 mb) is zonally averaged, it is able to explain about 30% of the common interannual variability in the whole forced simulation and just 15% of the common interannual variability in the control run. It seems therefore, that the variations in the solar insolation may be at least partially responsible for the contrasting meridional temperature gradients near the surface and at 200 mb, although this simultaneous anomaly pattern also appears, albeit less frequently, in the control simulation. It is noteworthy that a climate simulation with the ECHAM model (coupled to the ocean model OPYC) for the next 100 years with increasing concentrations of greenhouse gases shows a increasing Arctic Oscillation index (Zorita and González-Rouco, 2000).

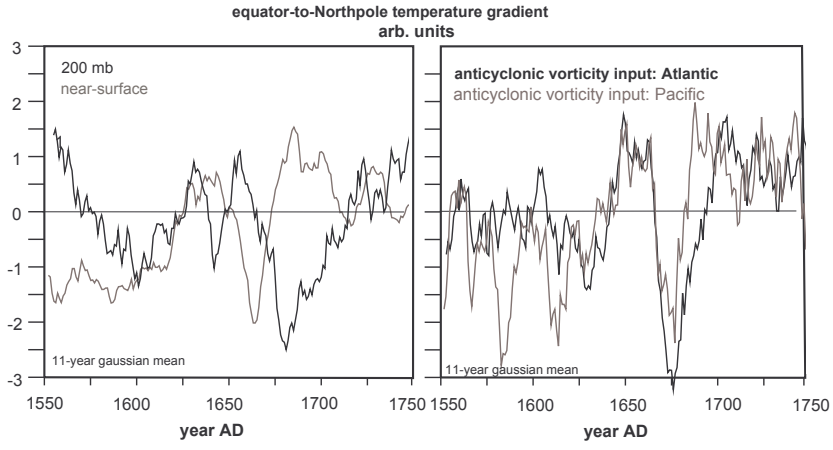

Figure 13: Zonally averaged annual equator-to-pole temperature gradient in the North Hemisphere at 200 mb height compared to the annual wind stress vorticity (positive, anticyclonic) averaged over the ocean grid-points in the North Atlantic and North Pacific basins. Anomalies are relative to the long-term mean 1550-1850 A.D.. Time series are normalized by their own standard deviation.

We now shortly explore other possible oceanic mechanism that may be involved in the negative temperature anomalies in the northernhigh latitudes in the LMM in the North Atlantic basin, namely deep water production in the North Atlantic. Fig.11c indicates that salinity at 100 m depth was lower than on the long-term mean in most of the North Atlantic ocean. This could be an indication of reduced water densities in the near-surface layers, conductive to a reduced oceanic convection in the North Atlantic at high latitudes. The variations in oceanic convective activity in the North Atlantic do show some connection with the LMM. Figure 14a shows the time series of the potential energy released in convective events, averaged in the Northern Seas at high latitudes and the time series of the averaged salinity at 100 m depth, also spatially averaged in the North Atlantic at high latitudes. For comparison purposes this figure also shows the intensity of the Gulf Stream, as defined previously. The evolution of the convective activity precedes the variations of salinity and of the strength of the Gulf Steam in the LMM, so that it would be suggestive to think that the convective activity is also contributing to variations of the Gulf Stream intensity. However, the variations of salinity seem to be just a response of either convective activity and/or variations in the intensity of the Gulf Stream. Also, the amplitude of the variations in the convective activity before and during the LMM are large, but not exceptional, whereas the anomalies of the Gulf Stream intensity and the wind-stress forcing reach outstanding levels in these decades. Similar conclusions can be drawn regarding

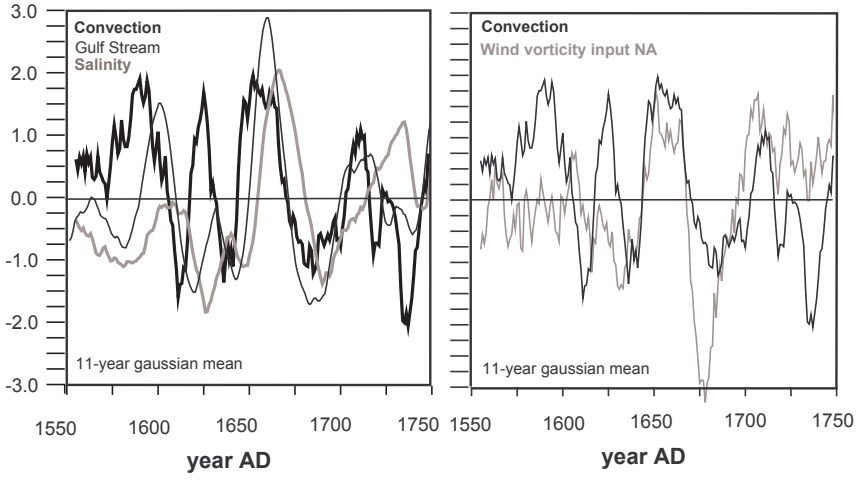

Figure 14: Top: annual potential energy released in oceanic convective events averaged over the high latitude North Atlantic and Nordic Seas; annual salinity at 100 m depth averaged over the high-latitude North Atlantic together with the Gulf Stream intensity indicator of Figure 12; Bottom: Ocean convective activity in the North Atlantic (as in top) together with the wind-stress vorticity input into the North Atlantic ocean. Anomalies are relative to the long-term mean 1550-1850 A.D.. Time series are normalized by their own standard deviation.

sea-surface temperature in the North Atlantic, since salinity and temperature evolve around the LMM in phase, as it could be expected by an advective mechanism. The question remains as to what are the origins of the variations in the convective activity. The ice cover anomalies south of Greenland throughout the LMM are locally formed and do not seem to be a result of ice advection from the Arctic along the Greenland coast. This is shown in selected snapshots with the LMM of the simulation in figure 15. In this figure the corresponding anomalies of convective activity are also shown. The ice cover anomalies are closely anticorrelated, in time and space, to anomalies of convective activity, indicating that probably the upward oceanic heat flux is locally driving the ice formation. The sea-surface salinity anomalies themselves do not seem to be large enough to influence decisively the formation of ice, since a reduction of 0.2 psu is linked to an increase of just 0.01 K in the freezing point of sea-water. An interesting aspect of the climate variations around the LMM is the recovery of the zonal circulation, and therefore of the anticyclonic vorticity input, to positive values before the LMM actually finished. This is consistent with the trend of the NAO index also seen in all empirical reconstructions (Fig. 6). This is also clearly seen in Figure 14b, where the simulated vorticity input becomes anticyclonic before 1700 A.D., while the solar radiation has barely recovered and the global temperature minimum has not yet occurred. Also clear is the decoupling of the vorticity input in the North Atlantic and North

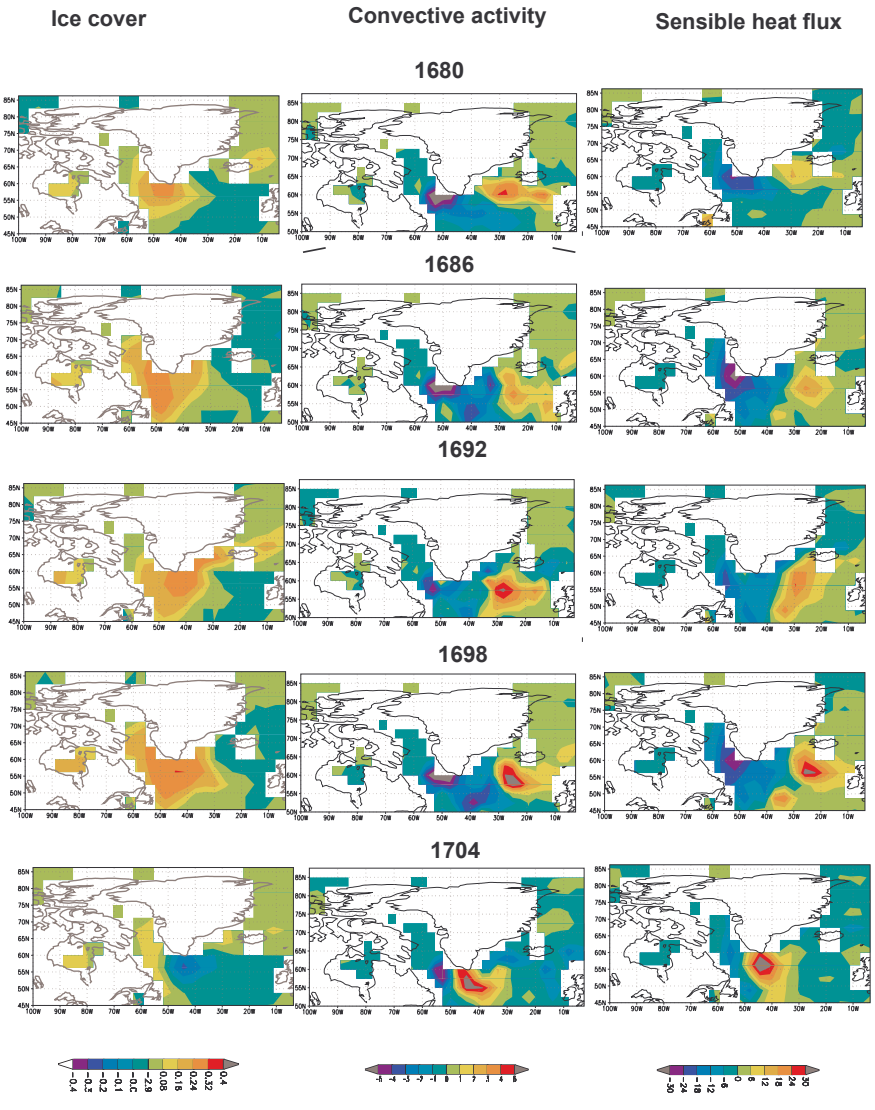

Figure 15: Anomalies of annual sea-ice cover, potential energy released by oceanic convection (watt/m^2)and sensible heat flux (watt/m^2,positive into the atmosphere) through the Late Maunder Minimum in the North Atlantic. The fields have been previously smoothed in time with a 5-year running mean filter.

Pacific basins from the temperature gradient at 200 mb at the outset of the LMM around 1700 A.D. (Fig. 13). A speculative mechanism that may explain this behavior is the reaction of the atmospheric circulation to the sea-surface-temperatures anomaly pattern created during the first stages in the LMM. Due to the weakening of the Western Boundary currents (and of the convective activity in the North Atlantic) the meridional temperature gradient is increased and this could possibly tend to intensify the atmospheric zonal circulation, i.e. a negative feedback to the original forcing. After some lag this negative feedback would overshoot and tend to bring

the advective negative SST anomalies at high latitudes to an end. This mechanism can only be ascertain by additional stand-alone experiments with the atmospheric submodel forced by LMM ocean surface fluxes. In general simulations with atmospheric GCMs driven by SST anomalies have not yielded a clear picture of the response of the atmospheric circulation. However, during the LMM the model simulated extensive sea-ice cover anomalies in the North Atlantic that allow for much lower surface temperatures and reduced heat-flux from the ocean (Figure 15).

The broad picture that emerges from this analysis is, therefore, that variations in the solar insolation around the LMM influence the atmospheric circulation, initially favoring a low zonal index. The reduced anticyclonic vorticity wind forcing associated to a low zonal index modulates the Western Boundary currents and in the North Atlantic possibly the intensity of oceanic convection, intensifying the sea-surface temperature and salinity drop at higher latitudes, specially in the North Atlantic. The recovery of the solar insolation to long-term values should bring these climate anomalies to an end, but the present climate simulations also suggest a possible negative feedback of the associated oceanic heat flux anomalies to the atmospheric circulation, that may react by increasing the zonal circulation and accelerating the Western Boundary Currents again, thereby contributing to a shortening of the LMM at high latitudes in both ocean basins.

6 Conclusions

The climate simulation described in the previous section represents a contribution to the reconstruction of the climate of the last centuries, complementary to the climate reconstructions derived from the analysis of proxy data. Of course, to gain a more conclusive picture , simulations with other climate models will have to be carried out and analyzed.

From this simulation several conclusions can be derived. Perhaps the most important is that the level of externally forced climate variability are larger than in most of the empirical climate reconstructions, and tends to agree, although not perfectly, with the reconstructions that indicate quite cold conditions throughout the Little Ice Ice and a steeper temperature recovery towards the 20^{th} century (Esper et al., 2002; Huang et al., 2000). In particular the temperature trends simulated at the recovery from the LMM are comparable to the simulated and observed temperature trends since the beginning of the industrialization. Therefore, from the model point of view, the 20^{th} global temperature trends are not unprecedented. This is consistent with empirical reconstructions of European temperature (Luterbacher et al., 2003, personal communication).

The climate model ECHO-G also reacts more sensitively to variations in the radiative forcing than the energy balance model of Crowley (2000), although essentially the same external forcing has been used in both simulations. The sensitivity of the model ECHO-G is however reasonable when compared to the simulated temperature increase of the last 100 years and to the results of other models under IPCC scenarios of climate change. This different sensitivity to changes in the radiative forcing underlines the need of using coupled three dimensional models under transient forcing to better take into account feedback processes and changes in the ocean circulation.

The simulated temperature deviations in Europe around the Late Maunder Minimum agree reasonably well with high resolution empirical reconstructions, both indicating colder temperatures in Eastern and Central Europe than near the Atlantic coast. This fact supports to some extent the ability of climate models in simulating climate change at regional scales. However, the model simulated colder temperatures,almost globally, in the Late Maunder Minimum, a result that may be traced back to the reduced effective insolation. Therefore, a modification of the atmospheric or oceanic circulation would not be strictly necessary to explain colder conditions in particular regions, e.g. Europe. The climate model, however, simulates markedly colder temperatures in the North Atlantic at high latitudes and over Greenland, and to a lesser extent also in the North Pacific, that seem to require changes in the regional circulation patterns. Unfortunately, this point cannot be checked with the empirical reconstruction.

The analysis of the model simulations suggests that the cause for this intensification of the temperature anomalies lies in the weakening of the Western Boundary currents around the LMM, caused by a weakening of the wind-stress forcing, a reflection of the low state North Atlantic Oscillation, at least in the initial phase of the LMM. This result is consistent with the simulations by Shindell et al. (2001), and most empirical reconstructions. However, the model simulates a more complex evolution of the NAOI within the LMM than equlibrium simulations are able to represent. A comparison of empirical reconstructions of the strength, and specially of the timing, of the Gulf Stream and the Kuroshio current in the LMM would be in this regard quite interesting. Also transient simulations with other coupled models should support this connection between solar forcing and intensity of the Western Boundary current systems.

This climate model also simulates large ice cover and sea surface salinity around the LMM, that are reminiscent of the Great Salinity Anomaly observed in the North Atlantic around 1970 A.D.. In this simulation the ice cover anomalies are not the result of ice advection, as observed in other model simulations (Hall and Stouffer, 2001), but are created in situ by a reduced ocean

convection south of Greenland, the lower solar insolation, and also probably by a reduced heat flux advection by the Gulf Stream. The reduced salinity at the surface, also a consequence of a weakened Gulf Stream, should have only played a minor role in the production of ice-cover anomalies.

Acknowledgments. The German Climate Computing Center (DKRZ) and NEC provided technical support. The gridded European land-based temperature data from the 20^{th} century have been supplied by the Climate Impacts LINK Project (UK Department of the Environment Contract EPG 1/1/16). J. L. was supported by the Swiss NCCR climate program and F. G-R. partially by the Spanish CICYT (REN 2000-0786). The GKSS work was part of the "Climate in Historical Times" Strategic Project of the Helmholtz Society. Part of the analysis was performed in the SFB 512 of the University of Hamburg. B. Gardeike prepared some of the diagrams.

References

Alcoforado, MJ Nuñes MD, Garcia JC, Taborda JP (2000) Temperature and precipitation reconstruction in southern Portugal during the late Maunder Minimum (A.D. 1675-1715). The Holocene 10: 333-340.

Barriendos M (1997) Climatic variations in the Iberian Peninsula during the late Maunder Minimum (A.D. 1675-1715): An analysis of data from rogation ceremonies.The Holocene 7, 105-111.

Betrand C, Loutre MF, Crucifix M, Berger A (f02) Climate of the last millenium: a sensitivity study. Tellus 54A: 221-244.

Borisenkov YP (1994) Climatic and other natural extremes in the European territory of Russia in the late Maunder Minimum (1675-1715), in Frenzel B, Pfister C Glaser B (eds), Climatic trends and anomalies in Europe 1675-1715, Fischer, Stuttgart, pp. 83-94.

Brzdil R, Dobrovolny P, Chocholc B, Munzar J (1994) Reconstruction of the climate of Bohemia and Moravia in the period of 1675 to 1715 on the basis of written sources. In Frenzel B, Pfister C, Glaser B (eds), Climatic trends and anomalies in Europe 1675-1715, Gustav Fischer Verlag, Stuttgart, Jena, New York, pp. 110-121.

Briffa KR, Osborn TJ (2002) Blowing hot and cold. Science 295: 2227-2228.

Briffa KR, Jones PD, Schweingruber FH, Osborn TJ (1998) Influence of volcanic eruptions on Northern Hemisphere summer temperature over the past 600 years. Nature 393: 450-455.

Blunier T, Chappellaz JA, Schwander J , Stauffer B, Raynaud D (1995) Variations in atmospheric methane concentration during the Holocene epoch. Nature 374: 46-49.

Cook ER, D'Arrigo RD, Briffa KR (1998) A reconstruction of the North Atlantic Oscillation using tree-ring chronologies from North America and Europe. The Holocene 8: 9-17.

Cook ER, D'Arrigo RD, Mann ME (2002) A well verified, multiproxy reconstruction of the Winter North Atlantic Oscillation Index since A.D. 1400. J Clim 15: 1574-1764.

Cook E , Esper J (2002) Tree-ring chronologies and climate variability, response. Science 296: 848-849.

Cook ER, Meko DM, Stahle DW, Cleaveland MK (1999): Drought reconstructions for the continental United States. J Clim 12: 1145-1162.

Crowley TJ (2000) Causes of climate change over the past 1000 years. Science 289: 270-277.

Cubasch U , Hegerl GC , Voss R, Waszkewitz J, Crowley TC (1997): Simulation with an O-AGCM of the influence of variations of the solar constant on the global climate. Clim Dyn 13: 757-767.

Cubasch U, Voss R (2000) The influence of total solar irradiance on climate. Space Science Reviews 94: 185-198.

Cubasch U and coauthors In: Climate Change (2001): The Scientific Basis. Contribution of Working Group I to the Third Assessment Report of the Intergovernmental Panel on Climate Change.[Houghton, J T et al.] (2001) and references therein.

Giorgi F, Francisco R (2000): Uncertainties in regional climate change prediction: a regional analysis of ensemble simulations with the HADCM2 coupled AOGCM. Clim Dyn 16: 169-182.

Esper J, Cook ER , Schweingruber FH (2002) Low-frequency signals in long tree-ring chronologies for reconstructing past temperature variability. Science 295: 2250-2253.

Dunbar RB, Cole JE (1993) Coral Records of Ocean-Atmosphere Variability. NOAA Climate and Global Change Program. Special Report No.10, UCAR, Boulder, 37pp. .

Druffel ERM, Griffin S (1993) Large variations of surface ocean radiocarbon: evidence of circulation changes in the southwestern Pacific. J Geophys Res 98 : 20249-20259 .

Eddy J (1976) The Late Maunder Minimum. Science 192: 1189-1202.

Etheridge D , Steele LP, Langenfelds RL, Francey RJ, Barnola JM, Morgan VI, (1996) Natural and anthropogenic changes in atmospheric $CO_2$2 over the last 1000 years from air in Antarctic ice and firn. J Geophys Res 101: 4115-4128.

Frenzel B , Pfister C, Glaser B (eds), 1994: Climatic trends and anomalies in Europe 1675-1715, Fischer, Stuttgart, 479 pp.

Fritts HC, Lough JM (1985) An estimate of average annual temperature variations for North America, 1602-1961. Clim Change 7, 203-224.

Ge Q, Zheng J, Fang X, Man Z, Zhang X, Zhang P, Wang W-C (2003) Winter half-year temperature reconstructions for the Middle and Lower reaches of the Yellow River and Yangtze river during the past 2000 years. The Holocene, in press.

Glaser R (2001) Klimageschichte Mitteleuropas: 1000 Jahre Wetter, Klima, Katastrophen. Primus Verlag. Darmstadt, 227 pp.

Glueck M F, Stockton CW (2001) Reconstruction of the North Atlantic Oscillation, 1429-1983. Int J Climatol 21: 1453-1465.

Fyfe JC, Boer GJ, Flato GM (1999) The Arctic and Antarctic oscillations and their projected changes under global warming. Geophys Res Lett 26: 1601-1604.

Hall A, Stouffer RJ (2001) An abrupt climate event in a coupled ocean-atmosphere simulation without external forcing. Nature 409: 171-174.

Hastenrath S , Greischar L (2001) The North Atlantic oscillation in the NCEP-NCAR reanalysis. J Clim 14: 2404-2413.

Hegerl GC , Hasselmann K, Cubasch U , Mitchell JFB, Roeckner E, Voss R, Waszkewitz J (1997) Multi-fingerprint detection and attribution analysis of greenhouse gas, greenhouse gas-plus-aerosol and solar forced climate change. Clim Dyn 13: 613-634.

Holmgren K, Karlen W, Lauritzen SE, Lee-Thorp JA, Partridge TC, Piketh S , Repinski P, Stevenson C, Svanered O, Tyson PD (1999): A 3000-year high-resolution stalagmite-based record of paleoclimate for northeastern South Africa. The Holocene 9 (3): 295-309.

Huang SH , Pollack HN, Shen PY (2000) Temperature trends ever the past five centuries reconstructed from borehole temperatures. Nature 403: 756-758.

Jones PD, Briffa KR, Barnett TP, Tett SFB (1998) High-resolution palaeoclimatic records for the last millennium: interpretation, integration and comparison with General Circulation Model control-run temperatures. The Holocene 8: 455-471.

Jones PD, New M, Parker DE, Martin S , Rigor IG (1999) Surface air temperature and its changes over the past 150 years. Rev Geophys 37: 173-199.

Jones PD , Osborn TJ, Briffa KR (2001) The evolution of climate over the last millenium. Science 292: 662-667.

Lean J , Beer J , Bradley R (1995) Reconstructions of solar irradiance since 1610- implications for climate change. Geophys Res Lett 22: 3195-3198.

Koslowski G, Glaser R (1999) Variations in reconstructed ice winter severity in the Western Baltic from 1501 to 1995, and their implications for the north Atlantic oscillation. Clim Change 41: 175-191.

Legrand J -P, Le Goff M, 1992 Les observations mtorologiques de Louis Morin entre 1670 et 1713, in Direction de la Mtorologie Nationale, Monographie Nr. 6, Meteo-France, Trappes.

Legutke S, Voss R (1999) The Hamburg Atmosphere-Ocean Coupled Circulation Model ECHO-G. Technical Report No. 18, DKRZ, Hamburg.

Luterbacher J, Rickli R, Xoplaki E, Tinguely C, Beck C, Pfister C, Wanner H (2001) The Late Maunder Minimum (1675-1715) - A key period for studying decadal scale climatic change in Europe. Clim Change 49: 441-462 (2001)

Luterbacher J, Xoplaki E Dietrich D, Rickli R, Jacobeit J, Beck C, Gyalistras D, Schmutz C, Wanner H (2002a) Reconstruction of Sea Level Pressure fields over the Eastern North Atlantic and Europe back to 1500. Clim Dyn 18: 545-561

Luterbacher J , Xoplaki E, Dietrich D, Jones P D, Davies TD, Portis D, González-Rouco J F, von Storch H, Gyalistras D, Casty C, Wanner H (2002b) Extending North Atlantic Oscillation reconstructions back to 1500. Atmos Sci Lett 20: 114-124.

Mann ME , Bradley RS, Hughes MK (1999) Northern Hemisphere temperatures during the past millennium: Inferences, uncertainties, and limitations. Geophys Res Lett 26 : 759-762.

Mann ME , Bradley RS, Hughes MK (1998) Global-scale temperature patterns and climate forcing over the past six centuries. Nature 392 : 779-787.

Mann ME , Hughes MK (2002) Tree-ring chronologies and climate variability. Science 296: 848-848

Mann ME, Rutherford S, Bradley RS, Hughes MK, and Keimig FT (2003) Optimal surface temperature reconstructions using terrestrial borehole data. J Geophys Res, in press.

Manley G (1974) Central England temperatures - monthly means 1659 to 1973. Quart J Roy Meteor Soc 100: 389-405.

Mysak LA , Manak DK , Marsden RF (1990) Sea-ice anomalies observed in the Greenland and Labrador seas during 1901-1984 and their relation to an interdecadal Arctic climate cycle. Clim Dyn 5: 111-133.

Ogilvie AEJ (1996) Sea ice conditions off the coasts Iceland A. D. 1601-1850 with special reference to part of the Maunder Minimum period (1675-1715). AmS-Varia 25, Archaeological Museum of Stavanger, Norway, 9-12.

Pfister C , Brazdil R, Glaser R, Barriendos M, Camuffo D, Deutsch M , Dobrovolny P, Enzi S, Guidoboni E, Kotyza O, Militzer S, Racz L, Rodrigo FS (1999) Documentary evidence on climate in sixteenth-century Europe. Climatic Change 43: 55-110.

Quinn TM, Crowley TJ, Taylor FW, Henin C, Joannot P, Join Y (1998) A multicentury isotopic record from a New Caledonia coral: Interannual and decadal sea surface temperature variability in the southwest Pacific since 1657 A.D. Paleoceanography 13, 412-426 (1998).

Robertson A , Overpeck J, Rind D, Mosley-Thompson E, Zielinski G, Lean J, Koch D, Penner J, Tegen I, Healy R, 2001 Hypothesized climate forcing time series for the last 500 years. J Geophys Res 106 (D14): 14783-14803.

Shindell DT, Miller RL, Schmidt GA, Pandolfo L (1999) Simulation of recent northern winter climate trends by greenhouse-gas forcing. Nature 399: 452-455.

Shindell DT, Schmidt GA, Mann ME, Rind D, Waple A (2001) Solar forcing of regional climate change during the maunder minimum. Science 294: 2149-2152.

Schmutz C, Luterbacher J, Gyalistras D, Xoplaki E, Wanner H (2000) Can we trust proxy-based NAO index reconstructions? Geophys Res Lett 27 (8): 1135-1138.

Slonosky VC , Jones PD, Davies TD (2001) Instrumental pressure observations and atmospheric circulation from the 17th and 18th centuries: London and Paris Int J Climatol 21: 285-298.

Stocker TF (2002) North-south connections . Science 297: 1814-1815.

Stott P A , Tett SF B, Jones GS, Allen MR, Mitchell JF B, Jenkins GJ (2000) External control of 20th century temperature variations by natural and anthropogenic forcings. Science 15: 2133-2137.

Tyson PE, Karlen W, Holmgren K , Heiss GA (2000) The Little Ice Age and medieval warming in South African. S Afr J Sci, 96: 121-126.

van den Dool HM , Krijnen HJ , Schuurmans CJE (1978) Average winter temperatures at De Bilt (The Netherlands): years 1634-1977. Climatic Change , 1: 319-330.

van Engelen AFV, Buisman J , Ijnsen F (2001) A millennium of Weather, Winds and Water in the Low Countries. In: Jones P D et al. (eds) History and Climate: Memories of the Future? Kluwer Academic Press, New York, Boston, London, 101-124 (2001).

Ulbrich U , Christoph M (1999) A shift of the NAO and increasing storm track activity over Europe due to anthropogenic greenhouse gas forcing. Clim Dyn 15: 551-559.

Villalba R, Lara A, Boninsegna JA, Aravena JC, Roig F, Schmelter A, Delgado S, Wolodarsky A , Ripalta A (2002) Large-scale temperature changes across the southern Andes: 20th-century variations in the context of the past 400 years. Clim Change, submitted.

Wang S, Gong D, Zhu J (2001) Twentieth-century climatic warming in China in the context of the Holocene. The Holocene 11 (3): 313-321.

Wanner H , Pfister C, Bradzil R, Frich P, Frydendahl K, Johnsson T, Kington J, Lamb HH, Rosenorn S, Wishmane E (1995) Wintertime European circulation patterns during the Late Maunder Minimum cooling period (1675-1704). Theor Appl Climatol 51: 167-175.

Yang BA, Braeuning KR Johnson, Yafeng S (2002): General characteristics of temperature variations in China during the last two millenia. Geophys Res Lett 29 (9), doi 10.1029/2001GL014485.

Zorita E , González-Rouco F (2000) Disagreement between predictions of the future behavior of the Arctic Oscillation as simulated in two different climate models: implications for global warming. Geophys Res Lett 27: 1755-1758.

Zorita E , González-Rouco F (2002) Are temperature proxies adequate for North Atlantic oscillation reconstructions?. Geophys Res Lett 29: 48-1 - 48-4

Xoplaki E , Maheras P, Luterbacher J (2001) Variability of climate in Meridional Balkans during the periods 1675-1715 and 1780-1830 and its impact on human life. Clim Change 48: 581-615.